Adaptive Multiresolution Finite Volume Discretization of the Variational Multiscale Method. General Framework.

Wolfgang Dahmen, Thomas Gotzen,

Siegfried Müller and Roland Schäfer

Bericht Nr. 332 **November 2011**

Key words: Variational Multiscale Method, multiscale analysis, biorthogonal wavelets, finite volume scheme

AMS subject classifications: 76F65, 76M12, 65T60

Institut für Geometrie und Praktische Mathematik

RWTH Aachen

Templergraben 55, D–52056 Aachen (Germany)

Adaptive multiresolution finite volume discretization of the Variational Multiscale Method. General Framework.

By W. Dahmen, T. Gotzen, S. Müller AND R. Schäfer

Institut für Geometrie und Praktische Mathematik, RWTH Aachen
Templergraben 55, 52056 Aachen

In order to investigate turbulent phenomena in compressible flows the Variational Multiscale method is used. This method is usually applied to incompressible flows. In a first step, we derive the VMS method for the compressible Navier-Stokes equations. The resulting weak formulation of the flow equations is split into resolved and unresolved scales using multiresolution techniques based on biorthogonal wavelets. Since the in principle infinite-dimensional subspace of fluctuations is also discretized, it needs to be stabilized by additional dissipative terms. The compressible VMS method is then incorporated into an adaptive multiresolution finite volume solver, where grid adaptation is also performed by means of the multiresolution analysis.

---

1. Introduction

The investigation of turbulent phenomena in compressible flows at high Reynolds numbers using Direct Numerical Simulations (DNS) is restricted to simple configurations only, because of the wide range of relevant scales that have to be resolved. In case of more complex applications such as the interaction of a hypersonic flow field with an injection jet of cooling gas through single boreholes or slots, it will not be feasible to resolve all scales. For this purpose low parametric turbulence models seem not to be reliable and capable of dealing with strongly heterogeneous discretizations resulting from locally refined grids. Here recent developments of the Variational Multiscale (VMS) method [1, 2] and related Subgrid Scale Methods [3, 4] seem to be more suited. These methods can be considered as advanced Large Eddy Simulation Methods (LES) [5–8]. Although these methods have been applied almost exclusively to incompressible flows we will apply the VMS method here to compressible flows. The key idea of the VMS method is to use the projection to an ansatz space of given resolution instead of convolution-based smoothing. Then the weak formulation of the flow equations that is split into resolved and unresolved scales shows the influence of fluctuation residual on the large scales and vice versa. The in principle infinite-dimensional subspace of fluctuations is also discretized and, hence, has to be stabilized. For stabilization dissipative terms are used containing model parameters that depend nonlinearly on the gradients of the fluctuations. The choice of the model is not as sensitive as in the context of LES, because it only affects the scales that are of the magnitude of the resolved fluctuation scales. Thus the influence of the model on the entire range of resolved scales is reduced. Another principle advantage of the VMS method in comparison to classical LES approaches lies in the fact that the commutation error resulting from the filter and

the differentiation process near to walls can be avoided. As was investigated in [9] this error can be much stronger than usually expected. Nevertheless there remains some heuristic, for instance, in the choice of the ansatz spaces concerning the resolved large and small scales. A priori, it is not known whether the budget of degrees of freedom corresponding to the chosen discretization will be sufficient to capture the influence of the small scales on the macro scale. For this purpose, we need to estimate the effect of the fluctuations. Here multiscale techniques seem to be promising. In [10, 11] quantitative results have been obtained, where the action of a nonlinearity on different scales is investigated. In particular, these allow for rigorous estimates to reduce small scale contributions.

The objective of the present work is to combine different frameworks, namely, (i) the VMS method, (ii) the concept of biorthogonal wavelets and (iii) the finite volume discretization. In particular, we describe how to embed the VMS method into an adaptive multiresolution finite volume (FV) solver using multiresolution techniques based on biorthogonal wavelets. For this purpose, we first introduce in Section 2 a multilevel representation of the VMS method based on a multiresolution analysis (MRA) that is performed by means of biorthogonal wavelets. The MRA provides us in a natural way with a decomposition of the underlying spaces into finite subspaces corresponding to resolved coarse and fine scales as well as the infinite subspace corresponding to unresolved fine scales. This decomposition is then applied to the weak formulation of the compressible Navier-Stokes equations. Finally, the influence of the unresolved scales on the resolved scales is modeled using the Smagorinsky model. Details on the discretization and implementation are then presented in Section 3. Finally we conclude with open questions that will be subject of future work.

2. Multilevel Representation for Variational Multiscale Method

In order to derive the VMS method we assume that there exists a solution u of the underlying problem lying in some infinite-dimensional function space $\mathcal{H}$. In a first step, we perform in Section 2.1 a multiscale decomposition of this space by means of a MRA where $\mathcal{H}$ is decomposed in three subspaces corresponding to a finite range of resolved large and small scales, respectively, and an infinite range of unresolved small scales. In Section 2.2 the MRA is then applied to the weak formulation of the compressible Navier-Stokes equations that results in equations for the resolved scales. Here we proceed similarly as in [8] for the incompressible case. Since the unresolved small scales will cause instabilities, their influence on the resolved small scales has to be modeled. We would like to emphasize that we confine ourselves to a brief conceptual sketch. A more thorough description of the concepts is postponed to subsequent work.

2.1. *Multiresolution analysis*

For the derivation of the VMS method we introduce some infinite-dimensional Hilbert space $\mathcal{H}$ of functions endowed with the inner product $\langle \cdot, \cdot \rangle_{\mathcal{H}}$. We assume that there exists a multiresolution sequence which is a nested sequence of closed linear subspaces $S_l \subset \mathcal{H}$ of dimension N_l, i.e.,

$$\mathcal{S}_0 \subset \mathcal{S}_1 \subset ... \subset \mathcal{S}_l \subset \mathcal{S}_{l+1} \subset ... \subset \mathcal{H} \tag{2.1}$$

such that the multiresolution sequence is dense in $\mathcal{H}$, i.e.,

$$\text{clos}_{\|\cdot\|} \left(\bigcup_{l \in \mathbf{N}_0} \mathcal{S}_l \right) = \mathcal{H}. \tag{2.2}$$

Typically the subspaces $\mathcal{S}_l$ are associated with different discretization levels of increasing resolution, where the corresponding grids $\mathcal{G}_l$ are nested, i.e., $\mathcal{G}_l \subset \mathcal{G}_{l+1}$. Due to the nesting of the subspaces there exist complement spaces $\mathcal{W}_l$ such that

$$\mathcal{S}_{l+1} = \mathcal{S}_l \oplus \mathcal{W}_l, \quad \mathcal{S}_l = \mathcal{S}_0 \oplus \mathcal{W}_0 \oplus \mathcal{W}_1 \oplus ... \oplus \mathcal{W}_{l-1}. \tag{2.3}$$

These spaces are spanned by the basis of scaling functions $\Phi_l := \{\phi_{l,k} : k \in \mathcal{I}_l\}$ and the wavelet basis $\Psi_l := \{\psi_{l,k} : k \in \mathcal{J}_l\}$, respectively, i.e., $\mathcal{S}_l = \text{span}\,\Phi_l$ and $\mathcal{W}_l = \text{span}\,\Psi_l$.

Here we confine the discussion to uniformly stable Riesz bases, i.e., there exist constants $c,\ C > 0$ independent of l such that the collections $\{\Theta_l\}_{l\in\mathbf{N}_0}$ with $\Theta_l = \Phi_l$ or $\Theta_l = \Phi_l \cup \Psi_l$ satisfy the Riesz property

$$c\,\|\mathbf{u}\|_{l^2} \le \|\sum_k u_k\,\theta_{l,k}\|_{\mathcal{H}} \le C\,\|\mathbf{u}\|_{l^2}, \qquad \forall\,\mathbf{u} \in \mathbf{R}^{\#\Theta_l}, \tag{2.4}$$

cf. [12]. In particular, if Θ_l is an orthonormal system, then the Riesz property holds with "$=$" instead of "$\le$" and $c = C = 1$. Since the multiresolution sequence is assumed to be dense in $\mathcal{H}$, the Hilbert space is the closure of the *single-scale basis* $\Phi := \bigcup_{l\in\mathbf{N}_0} \Phi_l$. Furthermore, we assume that the *multiscale basis* $\Psi := \Phi_0 \cup \bigcup_{l\in\mathbf{N}_0} \Psi_l$ is also a Riesz basis for $\mathcal{H}$. Then according to Dahmen [13] there is another Riesz basis $\tilde{\Psi} := \tilde{\Phi}_0 \cup \{\tilde{\Psi}_l\}_{l\in\mathbf{N}_0}$ of $\mathcal{H}$ which is biorthogonal to Ψ, i.e., $\langle\Psi, \tilde{\Psi}\rangle_{\mathcal{H}} = \mathbf{I}$ and $u \in \mathcal{H}$ has the unique expansion

$$u = \sum_{k\in I_0} u_{0,k}\phi_{0,k} + \sum_{l\in\mathbf{N}_0}\sum_{k\in\mathcal{J}_l} d_{l,k}\psi_{l,k}, \tag{2.5}$$

where, in particular, the single-scale coefficients and wavelet coefficients are determined by

$$u_{l,k} := \langle u, \tilde{\phi}_{l,k}\rangle_{\mathcal{H}}, \quad d_{l,k} := \langle u, \tilde{\psi}_{l,k}\rangle_{\mathcal{H}}. \tag{2.6}$$

In the sequel, the bases Φ_l and Ψ_l are always referred to as *primal scaling functions* and *primal wavelets*, respectively. Analogously, the bases $\tilde{\Phi}_l$ and $\tilde{\Psi}_l$ are called the *dual scaling functions* and *dual wavelets*, respectively. In particular the following relations hold between the primal and dual setting, cf. [12],

$$\langle\Phi_l, \tilde{\Psi}_l\rangle_{\mathcal{H}} = \mathbf{0},\ \langle\Psi_l, \tilde{\Phi}_l\rangle_{\mathcal{H}} = \mathbf{0},\ \langle\Phi_l, \tilde{\Phi}_l\rangle_{\mathcal{H}} = \mathbf{I},\ \langle\Psi_l, \tilde{\Psi}_l\rangle_{\mathcal{H}} = \mathbf{I}, \tag{2.7}$$

$$\mathcal{S}_l \perp \widetilde{\mathcal{W}}_l := \text{span}\{\tilde{\Psi}_l\},\ \tilde{\mathcal{S}}_l := \text{span}\{\tilde{\Phi}_l\} \perp \mathcal{W}_l. \tag{2.8}$$

Note that the dual multiresolution sequence $\{\tilde{\mathcal{S}}_l\}_{l\in\mathbf{N}_0}$ is also a dense sequence of closed linear subspaces in $\mathcal{H}$.

By means of the multiresolution sequence we now split the space $\mathcal{H}$ into the space $\bar{\mathcal{U}} := \mathcal{S}_{\bar{L}}$ of resolved large scales, the space $\mathcal{U}' := \mathcal{S}_{L'} \backslash \mathcal{S}_{\bar{L}} = \mathcal{W}_{\bar{L}} \oplus ... \oplus \mathcal{W}_{L'-1}$ of fluctuations corresponding to resolved small scales and the space $\hat{\mathcal{U}} := \mathcal{H} \backslash \mathcal{S}_{L'}$ of unresolved small scales, i.e.,

$$\mathcal{H} = \bar{\mathcal{U}} \oplus \mathcal{U}' \oplus \hat{\mathcal{U}}, \tag{2.9}$$

see Figure 1.

Note that the space $\bar{\mathcal{U}}' := \bar{\mathcal{U}} \oplus \mathcal{U}'$ of all resolved scales is finite whereas the space $\hat{\mathcal{U}}$ of all unresolved scales is infinite. In order to distinguish between the functions of the different function spaces, we introduce the convention $u \in \mathcal{H}$, $\bar{u} \in \bar{\mathcal{U}}$, $u' \in \mathcal{U}'$, $\bar{u}' \in \bar{\mathcal{U}}'$

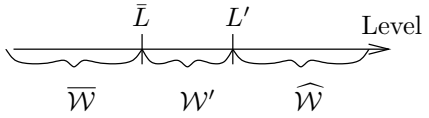

FIGURE 1. Splitting of function space $\mathcal{H}$ w.r.t. primal ($\mathcal{W} = \mathcal{U}$) and dual ($\mathcal{W} = \mathcal{V}$) system.

and $\hat{u} \in \hat{\mathcal{U}}$. From (2.5) we deduce the multiscale representation of these functions

$$\bar{u}' = \sum_{k \in \mathcal{I}_{L'}} u_{L',k}\, \phi_{L',k} = \bar{u} + u', \quad \bar{u} = \sum_{k \in \mathcal{I}_{\bar{L}}} u_{\bar{L},k}\, \phi_{\bar{L},k}, \quad u' = \sum_{l=\bar{L}}^{L'-1} \sum_{k \in \mathcal{J}_l} d_{l,k}\, \psi_{l,k}. \tag{2.10}$$

In a similar way we now proceed with the dual system

$$\mathcal{H} = \bar{\mathcal{V}} \oplus \mathcal{V}' \oplus \hat{\mathcal{V}}, \tag{2.11}$$

with $\bar{\mathcal{V}} := \tilde{\mathcal{S}}_{\bar{L}}$ the space of resolved large scales, $\mathcal{V}' := \tilde{\mathcal{S}}_{L'} \backslash \tilde{\mathcal{S}}_{\bar{L}} = \widetilde{\mathcal{W}}_{\bar{L}} \oplus ... \oplus \widetilde{\mathcal{W}}_{L'-1}$ the space of fluctuations corresponding to resolved small scales and $\hat{\mathcal{V}} := \mathcal{H} \backslash \tilde{\mathcal{S}}_{L'}$ the space of unresolved small scales. In analogy to (2.10) we obtain a multiresolution representation for the functions $v \in \mathcal{H}$, $\bar{v} \in \bar{\mathcal{V}}$, $v' \in \mathcal{V}'$, $\bar{v}' \in \bar{\mathcal{V}}'$ and $\hat{v} \in \hat{\mathcal{V}}$, where we change the role of the primal and dual system, i.e.,

$$\bar{v}' = \sum_{k \in \mathcal{I}_{L'}} \tilde{v}_{L',k}\, \tilde{\phi}_{L',k} = \bar{v} + v', \quad \bar{v} = \sum_{k \in \mathcal{I}_{\bar{L}}} \tilde{v}_{\bar{L},k}\, \tilde{\phi}_{\bar{L},k}, \quad v' = \sum_{l=\bar{L}}^{L'-1} \sum_{k \in \mathcal{J}_l} \tilde{d}_{l,k}\, \tilde{\psi}_{l,k}, \tag{2.12}$$

with dual single-scale coefficients and dual wavelet coefficients

$$\tilde{v}_{l,k} := \langle v, \phi_{l,k} \rangle_{\mathcal{H}}, \quad \tilde{d}_{l,k} := \langle v, \psi_{l,k} \rangle_{\mathcal{H}}. \tag{2.13}$$

2.2. *VMS method for compressible Navier Stokes equations*

In order to derive the VMS method, it is convenient to start with the weak formulation of the compressible Navier-Stokes equations

$$\begin{aligned} A(U, \phi_\rho) &:= \langle \rho_t, \phi_\rho \rangle_\Omega + \langle \nabla \cdot (\rho v), \phi_\rho \rangle_\Omega = 0, \\ B(U, \phi_m) &:= \langle (\rho v)_t, \phi_m \rangle_\Omega + \langle \nabla \cdot (\rho v \otimes v + pI), \phi_m \rangle_\Omega - \langle \nabla \cdot \sigma, \phi_m \rangle_\Omega = 0, \\ C(U, \phi_\mathcal{E}) &:= \langle (\rho E)_t, \phi_\mathcal{E} \rangle_\Omega + \langle \nabla \cdot ((\rho E + p) v), \phi_\mathcal{E} \rangle_\Omega - \langle \nabla \cdot (\sigma v + \lambda \nabla T), \phi_\mathcal{E} \rangle_\Omega = 0, \end{aligned} \tag{2.14}$$

where the L^2-inner product in the domain $\Omega \subset \mathbf{R}^d$ is defined as usual

$$\langle f, \phi \rangle_\Omega := \int_\Omega f\, \phi \, \mathrm{d}x. \tag{2.15}$$

The physical quantities are density ρ, velocity v, mass specific internal energy e and total energy $E = e + 0.5\, v^2$, pressure p and temperature T. The components of the shear stress tensor σ and the rate-of-deformation tensor S are determined by $\sigma_{ij} := \mu(2S_{ij} - \frac{2}{3} S_{kk} \delta_{ij})$ and $S_{ij} := \frac{1}{2}(\frac{\partial v_i}{\partial x_j} + \frac{\partial v_j}{\partial x_i})$, respectively. This system is closed by the equations of state for a calorically perfect gas

$$p = \rho R T, \qquad e = c_v T \tag{2.16}$$

with specific gas constant R and constant specific heats c_v and c_p.

The equations (2.14) represent the balance equations of continuity, momentum and

energy. Therefore it is natural to choose for the state vector the conserved quantities, i.e., $U = (\rho, \rho v, \rho E) = (\rho, m, \mathcal{E}) \in \mathcal{H}_\rho \times \mathcal{H}_m \times \mathcal{H}_\mathcal{E}$. For these quantities we have to choose appropriate Hilbert spaces $\mathcal{H}_\rho$, $\mathcal{H}_m$ and $\mathcal{H}_\mathcal{E}$ and associated inner products $\langle\cdot,\cdot\rangle_{\mathcal{H}_\rho}$, $\langle\cdot,\cdot\rangle_{\mathcal{H}_m}$ and $\langle\cdot,\cdot\rangle_{\mathcal{H}_\mathcal{E}}$ as ansatz spaces and test spaces. For the test functions we choose the same function spaces, i.e., $\phi = (\phi_\rho, \phi_m, \phi_\mathcal{E}) \in \mathcal{H}_\rho \times \mathcal{H}_m \times \mathcal{H}_\mathcal{E}$, but we will later on employ the basis corresponding to the dual system in Section 2.1. Note that the choice of the function spaces is not yet clear and typically they are not specified in the literature, cf. [8, 16]. In the following we will confine to the classical L^2-setting, i.e., $\mathcal{H}_\rho, \mathcal{H}_m, \mathcal{H}_\mathcal{E} \subset L^2(\Omega)$ associated with the L^2-inner product. Note, however, that in principle we need more regularity in view of the gradients involved in the weak formulation (2.14). Although we postpone a detailed discussion of this issue to future investigations, it is nevertheless important, because it might have a significant influence on the scaling of the equations and, hence, on the model to be specified below. Furthermore, the system (2.14) has to be complemented with boundary conditions also given in a weak formulation. Since the modeling procedure is similar for these terms, we omit the details here.

In a first step towards the VMS method, we split each of the components of the state vector U into the resolved part $\bar{U}' = \bar{U} + U'$ composed of the large scales $\bar{U}$ and the resolved small scales U', and the unresolved part $\hat{U} = U - \bar{U}'$ of unresolved small scales, i.e., $U = \bar{U} + U' + \hat{U}$. For this purpose, we apply the decomposition (2.9) corresponding to the *primal* system of the function space $\mathcal{H}$ representing either of the spaces $\mathcal{H}_\rho$, $\mathcal{H}_m$ and $\mathcal{H}_\mathcal{E}$. Plugging this decomposition into (2.14) and splitting the integrals into purely resolved scales and mixed terms of resolved and unresolved scales we obtain the equivalent weak formulation

$$\begin{aligned} A(\bar{U}', \phi_\rho) + A_1(\hat{U}, \phi_\rho) &= 0, \\ B(\bar{U}', \phi_m) + B_1(\bar{U}', \hat{U}, \phi_m) + B_2(\hat{U}, \hat{U}, \phi_m) &= 0, \\ C(\bar{U}', \phi_\mathcal{E}) + C_1(\bar{U}', \hat{U}, \phi_\mathcal{E}) + C_2(\hat{U}, \hat{U}, \phi_\mathcal{E}) &= 0, \end{aligned} \tag{2.17}$$

where the mixed terms are defined below. In order to account for the nonlinear dependence of the primitive variables on the conserved variables, we introduce Favre averaged quantities, where for each quantity $f = f(U)$ that depends nonlinearly on the state vector U we define

$$\bar{f} := f(\bar{U}), \quad \bar{f}' := f(\bar{U}'), \quad f' := f(\bar{U}') - \bar{f}, \quad \hat{f} := f(U) - \bar{f}'. \tag{2.18}$$

Note that due to the nonlinearity $\overline{f(U)} \neq f(\bar{U})$. In particular, we apply the Favre averaging to the velocity, the pressure, the shear stress and the temperature, i.e., $f \in \{v = m/\rho, p, \sigma, T\}$. Then the mixed terms in (2.17) are defined by

$$\begin{aligned} A_1(\hat{U}, \phi_\rho) :=& \langle \hat{\rho}_t, \phi_\rho \rangle_\Omega + \langle \nabla \cdot \hat{m}, \phi_\rho \rangle_\Omega = A(\hat{U}, \phi_\rho), \\ B_1(\bar{U}', \hat{U}, \phi_m) :=& \langle \hat{m}_t, \phi_m \rangle_\Omega + \langle \nabla \cdot (\hat{m} \otimes \bar{v}' + \bar{m}' \otimes \hat{v}), \phi_m \rangle_\Omega + \langle \nabla \cdot (\hat{p} I), \phi \rangle_\Omega \\ & - \langle \nabla \cdot \hat{\sigma}, \phi_m \rangle_\Omega, \\ B_2(\hat{U}, \hat{U}, \phi_m) :=& \langle \nabla \cdot (\hat{m} \otimes \hat{v}), \phi \rangle_\Omega, \\ C_1(\bar{U}', \hat{U}, \phi_\mathcal{E}) :=& \langle \hat{\mathcal{E}}_t, \phi_\mathcal{E} \rangle_\Omega + \langle \nabla \cdot (\hat{\mathcal{E}} \bar{v}' + \overline{\mathcal{E}}' \hat{v}), \phi_\mathcal{E} \rangle_\Omega + \langle \nabla \cdot (\hat{p} \bar{v}' + \bar{p}' \hat{v}), \phi_\mathcal{E} \rangle_\Omega \\ & - \langle \nabla \cdot (\hat{\sigma} \bar{v}' + \bar{\sigma}' \hat{v} + \lambda \nabla \hat{T}), \phi_\mathcal{E} \rangle_\Omega \\ C_2(\hat{U}, \hat{U}, \phi_\mathcal{E}) :=& \langle \nabla \cdot (\hat{\mathcal{E}} \hat{v}), \phi_\mathcal{E} \rangle_\Omega + \langle \nabla \cdot (\hat{p} \hat{v}), \phi_\mathcal{E} \rangle_\Omega + \hat{\sigma} \hat{v}. \end{aligned} \tag{2.19}$$

In a second step we also split the test function $\phi \in \mathcal{H}$ into three parts according to the decomposition (2.11) of the *dual* system, i.e., $\phi = \bar{\phi} + \phi' + \hat{\phi}$, where ϕ represents either of the three functions $\phi_\rho \in \mathcal{H}_\rho$, $\phi_m \in \mathcal{H}_m$ and $\phi_\mathcal{E} \in \mathcal{H}_\mathcal{E}$. Due to the linearity of the weak formulation (2.17) with respect to the test functions we may separate the equations for the different scales, where the test is performed for either $\bar{\phi}$, ϕ' or $\hat{\phi}$. Since we do not want to solve the equations for the unresolved small scales $\hat{\phi}$, we drop these equations. Therefore we have to model the influence of the unresolved scales on the resolved scales. For this purpose we make the following assumptions:

Assumption 1 The interaction of the resolved scales with the unresolved scales has no effect on the resolved scales, i.e.,

$$A_1(\bar{U}', \hat{U}, \bar{\phi}'_\rho) \approx 0,\ B_1(\bar{U}', \hat{U}, \bar{\phi}'_m) \approx 0,\ C_1(\bar{U}', \hat{U}, \bar{\phi}'_\mathcal{E}) \approx 0. \tag{2.20}$$

This assumption is typically employed in the RANS methodology and is only valid if a spectral gap in the occurring scales exists.

Assumption 2 The influence of the small-small interactions has a negligible effect on the resolved large scales, i.e.,

$$B_2(\hat{U}, \hat{U}, \bar{\phi}_m) \approx 0,\ C_2(\hat{U}, \hat{U}, \bar{\phi}_\mathcal{E}) \approx 0, \tag{2.21}$$

and their influence on the resolved small scales can be modeled, i.e.,

$$B_2(\hat{U}, \hat{U}, \phi'_m) \approx SB(U', \phi'_m),\ C_2(\hat{U}, \hat{U}, \phi'_\mathcal{E}) \approx SC(U', \phi'_\mathcal{E}). \tag{2.22}$$

With these assumptions the infinite system (2.17) including all scales then finally reduces to the approximate finite VMS method

$$A(\bar{U}', \bar{\phi}'_\rho) = 0,\ B(\bar{U}', \bar{\phi}'_m) + SB(U', \phi'_m) = 0,\ C(\bar{U}', \bar{\phi}'_\mathcal{E}) + SC(U', \phi'_\mathcal{E}) = 0. \tag{2.23}$$

Here the turbulence model is chosen as the Smagorinsky model, cf. [16], where the small-scale Reynolds stress and the small-scale Reynolds enthalpy flux are replaced by

$$SB(U', \phi'_m) := -\langle \nabla \cdot \sigma', \phi'_m \rangle_\Omega = -\langle \nabla \cdot \sigma', \bar{\phi}'_m \rangle_\Omega + \langle \nabla \cdot \sigma', \bar{\phi}_m \rangle_\Omega, \tag{2.24}$$

$$SC(U', \phi'_\mathcal{E}) := -\langle \nabla \cdot (\lambda'_t \nabla T'), \phi'_\mathcal{E} \rangle_\Omega = -\langle \nabla \cdot (\lambda'_t \nabla T'), \bar{\phi}'_\mathcal{E} \rangle_\Omega + \langle \nabla \cdot (\lambda'_t \nabla T'), \bar{\phi}_\mathcal{E} \rangle_\Omega, \tag{2.25}$$

where the quantities of the fluctuations are defined by

$$\sigma'_{ij} := \mu'_t \big(2S'_{ij} - \frac{2}{3} S'_{kk} \delta_{ij}\big), \quad S'_{ij} := \frac{1}{2}\Big(\frac{\partial v'_i}{\partial x_j} + \frac{\partial v'_j}{\partial x_i}\Big), \tag{2.26}$$

$$\mu'_t := \bar{\rho}(C'_s \Delta')^2 |S'|, \quad |S'| := \sqrt{2 S'_{ij} S'_{ij}}, \quad C'_s := 0.1, \tag{2.27}$$

$$\lambda'_t := c_p \mu'_t / Pr_t, \tag{2.28}$$

and Δ' denotes the local grid size, e.g., the cubic root of the volume of the test functions' support. The subgrid-scale Prandtl number Pr_t is assumed to be constant, where for our computations we use $Pr_t = 0.9$. It is known from literature that the Smagorinsky model works quite well for isotropic, homogeneous, fully developed turbulence, cf. [17].

Note that in the classical LES approach the modeling acts on all resolved scales, whereas in the VMS approach (2.23) it only acts on the resolved small scales.

3. Discretization of the Variational Multiscale Method

For a compact presentation of the VMS method we rewrite (2.23), (2.24) and (2.25) in vector representation

$$\langle \bar{U}'_t, \bar{\phi}' \rangle_\Omega + \langle \nabla \cdot F^I(\bar{U}'), \bar{\phi}' \rangle_\Omega - \langle \nabla \cdot F^D(\bar{U}'), \bar{\phi}' \rangle_\Omega - \langle \nabla \cdot F^S(U'), \phi' \rangle_\Omega = 0 \tag{3.1}$$

with the inviscid flux F_I, the dissipative flux F_D and the model flux F_S defined by

$$F^I(\bar{U}') = (\rho v, \rho v \otimes v + p\, I, \rho v(E + p/\rho)), \tag{3.2}$$

$$F^D(\bar{U}') = (0, \sigma, \sigma \cdot v + \lambda \nabla T),\ F^S(U') = (0, \sigma', \lambda' \nabla T'). \tag{3.3}$$

Here we introduce the vector inner product $\langle U, \phi \rangle_\Omega := (\langle u_\rho, \phi_\rho \rangle_\Omega, \langle u_m, \phi_m \rangle_\Omega, \langle u_\mathcal{E}, \phi_\mathcal{E} \rangle_\Omega)$. Since the weak formulation (3.1) is operating on function spaces, a natural discretization would be based on these spaces. Therefore the Discontinuous Galerkin (DG) method would be most convenient. However we want to embed the VMS method in the adaptive multiresolution solver Quadflow [18] that is based on a FV discretization operating on discrete data. Recently, Gravemeier [8] realized the VMS method for the *incompressible* Navier-Stokes equations using a FV method. Basically we follow this approach, but we employ the multiscale analysis in Section 2.1. In particular, the MRA for the ansatz space will be employed to perform grid adaptation and, thus, to improve the efficiency of the resulting scheme.

3.1. *Multiresolution analysis on* L^2

When it comes to the discretization of (3.1) we have to specify the ansatz and test spaces and their bases. As already mentioned above, we choose $\mathcal{H} = L_2(\Omega)$ equipped with the standard L^2-inner product for each of the ansatz and test spaces. In the following we summarize the basic ingredients for the construction of an appropriate MRA according to Section 2.1 using biorthogonal wavelets. Starting point is a hierarchy of nested grids $\mathcal{G}_l := \{V_{l,k}\}_{k \in \mathcal{I}_l}$ corresponding to different resolution levels $l \in \mathbf{N}_0$, where the mesh size decreases with increasing refinement level. This implies that each cell $V_{l,k}$ on level l is the union of cells $V_{l+1,r}$ on the next higher refinement level $l+1$, i.e.,

$$V_{l,k} = \bigcup_{r \in \mathcal{M}^0_{l,k}} V_{l+1,r}, \tag{3.4}$$

where $\mathcal{M}^0_{l,k} \subset I_{l+1}$ is the refinement set. Since we are aiming at a FV discretization, we associate with each cell $V_{l,k}$ in the partitions $\mathcal{G}_l$ the *box function*

$$\tilde{\phi}_{l,k}(x) := \frac{1}{|V_{l,k}|} \chi_{V_{l,k}}(x) = \begin{cases} 1/|V_{l,k}| & , \quad x \in V_{l,k} \\ 0 & , \quad x \notin V_{l,k} \end{cases}, \quad k \in \mathcal{I}_l \tag{3.5}$$

defined as the L^1–normalized characteristic function of $V_{l,k}$. By $|V|$ we denote the volume of a cell V. Note that by this choice the single-scale coefficients defined in (2.6) coincide with the cell average of the function u. Obviously, the nestedness of the grids as well as the linearity of integration imply the two–scale relations

$$\tilde{\phi}_{l,k} = \sum_{r \in \mathcal{M}^0_{l,k}} m^{l,0}_{r,k}\, \tilde{\phi}_{l+1,r}, \quad k \in \mathcal{I}_l, \tag{3.6}$$

of the box functions and the cell averages defined in (2.6), where the mask coefficients turn out to be $m^{l,0}_{r,k} := |V_{l+1,r}|/|V_{l,k}|$.

To the system $\tilde{\Phi}_l$ of box functions, we introduce the wavelet functions $\tilde{\psi}_{l,k}$ as linear

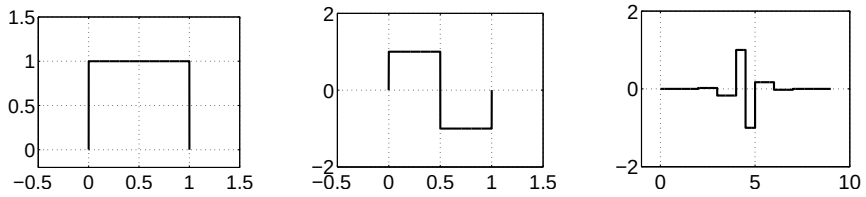

FIGURE 2. Box function $\tilde{\phi}$ (left), Haar wavelet $\tilde{\psi}^B$ (middle), and modified Haar wavelet $\tilde{\psi}^M$ with $M = 5$ vanishing moments (right), where all functions are defined on a reference element.

combinations of the box functions, i.e.,

$$\tilde{\psi}_{l,k} := \sum_{r \in \mathcal{M}^1_{l,k} \subset I_{l+1}} m^{l,1}_{r,k}\, \tilde{\phi}_{l+1,r}, \quad k \in \mathcal{J}_l, \tag{3.7}$$

with mask coefficients $m^{l,1}_{r,k}$ that only depend on the grids. The wavelet functions $\tilde{\Psi}_l := (\tilde{\psi}_{l,k})_{k \in \mathcal{J}_l}$ are assumed to build an appropriate completion of the basis system $\tilde{\Phi}_l$, i.e., the following three properties hold:

Efficiency: the wavelet functions are locally supported such that the support is uniformly bounded up to some constant C independent of l, i.e.,

$$|\text{supp}\, \tilde{\psi}_{l,k}| \leq C\, 2^{-ld}; \tag{3.8}$$

Cancellation: the wavelet functions have vanishing moments of order M, i.e.,

$$\langle P, \tilde{\psi}_{l,k} \rangle_\Omega = 0, \quad \forall\, P \in \Pi_{M-1}; \tag{3.9}$$

Stability: there exists a biorthogonal system Φ_l and Ψ_l of primal functions satisfying two-scale relations similar to (3.6) and (3.7). This is closely related to the Riesz basis property (2.4) of the infinite collection $\tilde{\Phi}_0 \cup \bigcup_{l=0}^{\infty} \tilde{\Psi}_l$ of $L_2(\Omega)$.

Aside from the above stability aspects, the biorthogonal framework allows for an efficient change of basis. While the relations (3.6) and (3.7) provide expressions of the coarse-scale box functions and detail functions as linear combinations of fine-scale box functions, the mask coefficients in the analogous two-scale relations for the dual system Φ_l, Ψ_l give rise to the reverse change of basis between $\tilde{\Phi}_l \cup \tilde{\Psi}_l$ and $\tilde{\Phi}_{l+1}$, i.e.,

$$\tilde{\phi}_{l+1,k} = \sum_{r \in \mathcal{G}^0_{l,k} \subset I_l} g^{l,0}_{r,k}\, \tilde{\phi}_{l,r} + \sum_{r \in \mathcal{G}^1_{l,k} \subset J_l} g^{l,1}_{r,k}\, \tilde{\psi}_{l,r}, \quad k \in I_{l+1}, \tag{3.10}$$

where we rewrite the basis function $\tilde{\phi}_{l+1,k}$ on level $l+1$ by the scaling functions $\tilde{\phi}_{l,r}$ and the wavelet functions $\tilde{\psi}_{l,r}$ on the next coarser scale l. Here again the mask coefficients $g^{l,0}_{r,k}$ and $g^{l,1}_{r,k}$ depend only on the grid geometry.

In the following we will briefly summarize the construction of two MRAs that both will be applied below for either the ansatz or the test space, respectively. The most simple one is the Haar basis corresponding to a Cartesian grid hierarchy. In [19] it was shown how to extend this basis to arbitrary nested grid hierarchies. For the construction the so-called box wavelets are introduced as a linear combination of the fine–scale box functions $\tilde{\phi}_{l+1,r},\ r \in \mathcal{M}^0_{l,k}$, related to the refinement of the cell $V_{l,k}$,

$$\tilde{\psi}^B_{l,k,e} := \sum_{r \in \mathcal{M}^0_{l,k}} a^{l,k}_{0,r} a^{l,k}_{e,r}\, \tilde{\phi}_{l+1,r}, \quad e \in E^* := E \backslash \{0\} \tag{3.11}$$

with $E := \{0, \ldots, M_r - 1\}$ and $M_r := \#\mathcal{M}^0_{l,k}$ the cardinality of the refinement set .

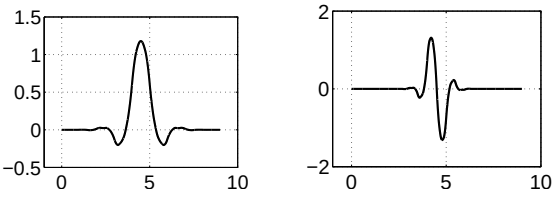

FIGURE 3. Primal scaling function ϕ^M (left) and primal wavelet ψ^M (right) corresponding to the modified Haar wavelet $\tilde{\psi}^M$ with $M = 5$ vanishing moments, where all functions are defined on a reference element.

Here the coefficients are determined such that the vectors $\mathbf{a}_e^{l,k} := (a_{e,r}^{l,k})_{r\in\mathcal{M}_{l,k}^0}$, $e \in E^*$, form an orthonormal system to the vector $\mathbf{a}_0^{l,k} := \left(\sqrt{|V_{l+1,r}|/|V_{l,k}|}\right)_{r\in\mathcal{M}_{l,k}^0}$. Then the system $\{\tilde{\phi}_{l,k}, \tilde{\psi}_{l,k,1}^B, \ldots, \tilde{\psi}_{l,k,M_r}^B\}$ of L^1-normalized functions is orthogonal to the system of L^∞-scaled functions $\{\phi_{l,k}, \psi_{l,k,1}^B, \ldots, \psi_{l,k,M_r}^B\}$ defined by $\phi_{l,k} := |V_{l,k}|\,\tilde{\phi}_{l,k}$ and $\psi_{l,k,e}^B := |V_{l,k}|\,\tilde{\psi}_{l,k,e}^B$. Obviously, the above design principles hold by construction, where the support of the box wavelets is $V_{l,k}$ and the order of vanishing moments is $M = 1$. In particular, we deduce the reverse change of basis (3.10) from the orthogonality of the parameter vectors

$$\tilde{\phi}_{l+1,r} = \tilde{\phi}_{l,k} + \sum_{e\in E^*} \frac{a_{e,r}^{l,k}}{a_{0,r}^{l,k}}\,\tilde{\psi}_{l,k,e}^B, \quad r \in \mathcal{M}_{l,k}^0. \tag{3.12}$$

Since later on we want to compress the test space, we need wavelets with higher vanishing moments that allow for higher compression rates. For this purpose, the box wavelet is not convenient. By means of a change of stable completion, cf. [12], we may deduce another MRA, where we introduce additional parameters of freedom by adding coarse-scale box functions to the box wavelets, i.e.,

$$\tilde{\psi}_{l,k,e}^M = \tilde{\psi}_{l,k,e}^B + \sum_{s\in\mathcal{L}_{l,k}} l_{l,k,e}^s\,\tilde{\phi}_{l,s},\ e \in E^*. \tag{3.13}$$

Here the index set $\mathcal{L}_{l,k} \subset I_l$ denotes a neighborhood of the cell $V_{l,k}$. Then the parameters $l_s^{l,k}$ can be determined by the cancellation property (3.9) solving a linear system of equations that in general will be underdetermined. The details of the construction can be found in [19]. Here we only want to remark that typically the dual wavelets $\tilde{\psi}_{l,k}^M$ are piecewise constant functions with vanishing moments of order M, whereas the primal wavelets $\psi_{l,k}^M$ in general are not known explicitly. However, they have some regularity, i.e., they are elements of some Hölder space C^s with $s \leq M$, cf. [20]. Moreover, we note that because of (3.5) the basis functions of the primal and dual system are normalized with respect to the L^∞- and L^1-metric, respectively.

For an example we consider the case of a 1D dyadic grid hierarchy. The primal and dual functions of the resulting MRAs can be deduced as translates and shifts of the generator functions of the scaling and wavelet function, respectively, presented in Figures 2 and 3. In particular, the box wavelet then coincides with the well-known Haar wavelet. Then the MRAs for multidimensional Cartesian grid hierarchies can be constructed using tensor products of these functions, cf. [19].

Finally, since a FV scheme is operating on the coefficients rather than the functions, we need to provide the two-scale relations (3.6), (3.7) and (3.10), respectively, in terms

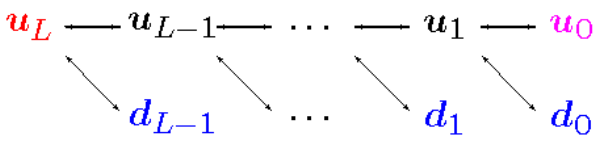

FIGURE 4. Pyramid scheme of multiscale transformation.

of the coefficients (2.6). For this purpose, we first note that because of $\langle\cdot,\cdot\rangle_{\mathcal{H}} = \langle\cdot,\cdot\rangle_{\Omega}$ and (3.5) the single-scale coefficients $u_{l,k}$ coincide with the cell averages of the underlying function u in the cell $V_{l,k}$. Then the nesting property (3.4) and the two-scale relations (3.6), (3.7) imply

$$u_{l,k} = \sum_{r\in\mathcal{M}^0_{l,k}} m^{l,0}_{r,k}\, u_{l+1,r}, k \in \mathcal{I}_l, \qquad d_{l,k} = \sum_{r\in\mathcal{M}^1_{l,k}} m^{l,1}_{r,k}\, u_{l+1,r},\ k \in \mathcal{J}_l, \tag{3.14}$$

and, reversely we conclude with (3.10)

$$u_{l+1,k} = \sum_{r\in\mathcal{G}^0_{l,k}} g^{l,0}_{r,k}\, u_{l,r} + \sum_{r\in\mathcal{G}^1_{l,k}} g^{l,1}_{r,k}\, d_{l,r}, \quad k \in I_{l+1}. \tag{3.15}$$

Successively applying these discrete two-scale relations, see Figure 4, we obtain a discrete analogon of (2.5).

3.2. *Finite volume discretization of the VMS method*

In order to discretize the VMS method (3.1) we choose for the decomposition of the ansatz and test space the primal and dual bases of the biorthogonal system corresponding to the MRAs formed by either the modified box wavelets or the box wavelets, see Section 3.1, respectively. This is sketched in Figure 5. In particular, each component of the state vector $\bar{U}'$ is a linear combination of the single-scale basis $\Phi^M_{L'}$ and, equivalently, of the multiscale basis $\Phi^M_0 \cup \bigcup_{l=0}^{L'-1} \Psi^M_l$ according to (2.10). In order to determine the coefficients $\{u_{L',k}\}_{k\in\mathcal{I}_{L'}}$ and $\{u_{0,k}\}_{k\in\mathcal{I}_0} \cup \bigcup_{l=0}^{L'-1}\{d_{l,k}\}_{k\in\mathcal{J}_l}$ we perform the test in (3.1) by the dual single-scale basis $\tilde{\Phi}^B_{L'}$ and dual multiscale basis $\tilde{\Phi}^B_0 \cup \bigcup_{l=0}^{L'-1} \tilde{\Psi}^B_l$, respectively.

Since we use the box function (3.5) for the test functions each component of $\bar{\phi}'$ in (3.1) is determined by

$$\bar{\phi}' = \tilde{\phi}_{L',k'}. \tag{3.16}$$

Moreover, their gradients vanish, because the box functions are constant inside their supports. Therefore we may rewrite the convective and viscous terms in (2.14) applying the Gaussian theorem as

$$\langle \bar{U}'_t, \bar{\phi}'\rangle_\Omega + \langle F^I(\bar{U}')\cdot n, \bar{\phi}'\rangle_{\bar{\Gamma}'} - \langle F^D(\bar{U}')\cdot n, \bar{\phi}'\rangle_{\bar{\Gamma}'} - \langle \nabla\cdot F^S(U'), \phi'\rangle_\Omega = 0. \tag{3.17}$$

Here n denotes the outer normal to the boundary $\bar{\Gamma}'$ of the test function's support. The L^2-inner product on a boundary Γ is defined similar to (2.15)

$$\langle f, \phi\rangle_\Gamma := \int_\Gamma f\,\phi\, \mathrm{d}S. \tag{3.18}$$

In the following we discuss how to discretize the integrals in (3.17):

Cell averages: First of all, we note that for both MRAs the dual scaling functions are determined by the box function (3.5), i.e., $\tilde{\Phi}^B_{L'} \equiv \tilde{\Phi}^M_{L'}$. By the biorthogonality property

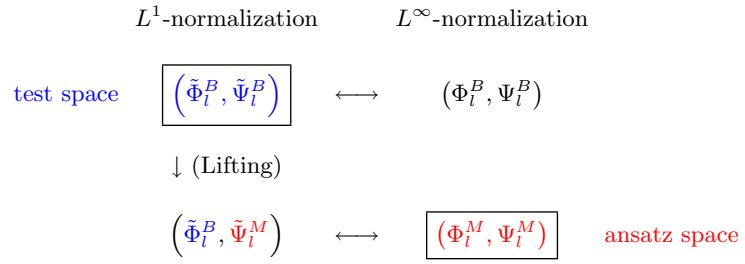

FIGURE 5. Construction of different MRAs as stable completions of box functions $\tilde{\Phi}_l^B$

(2.7) we then conclude with (2.10) and (3.16) that $\langle \bar{U}', \bar{\phi}' \rangle_\Omega = U_{L',k'}$, where $U_{L',k'}$ denotes the cell averages of the state vector $\bar{U}'$ corresponding to cell $V_{L',k'}$. Hence, the first volume integral in (3.17) coincides with the time derivative of the discrete cell averages for the conserved quantities, i.e.,

$$\langle \bar{U}'_t, \bar{\phi}' \rangle_\Omega = \frac{d}{dt} U_{L',k'}. \tag{3.19}$$

Flux approximation: Although the coefficients of the multiscale representation (2.10) are available by approximation, we cannot evaluate these representations, because the primal basis function corresponding to the MRA deduced from the modified box wavelets are in general not explicitly given. As is standard in the FV framework, we therefore replace $\bar{U}'$ on each cell $V_{L',k'}$ by some reconstruction polynomial $R_{L',k'} \in \Pi_q$ of degree q determined by the coefficients corresponding to the neighbor cells. Note that the reconstruction procedure is typically applied to the primitive variables ρ, v, p and T instead of the conserved quantities. The inviscid fluxes F^I are then approximated applying some approximate Riemann solver, whereas for the dissipative fluxes F^D we perform a weighted-averaging of the gradients of the reconstruction polynomials corresponding to the cells adjacent to the cell edge. Then the boundary integrals in (3.17) are approximated by

$$\langle F^I(\bar{U}') \cdot n, \bar{\phi}' \rangle_{\bar{\Gamma}'} \approx |V_{L',k'}|^{-1} B^I_{L',k'} := \sum_{j' \in \mathcal{N}(k')} |\Gamma^{L'}_{k'j'}| \, G^I(R_{L',k'}, R_{L',j'}, n_{k'j'}), \tag{3.20}$$

$$\langle F^D(\bar{U}') \cdot n, \bar{\phi}' \rangle_{\bar{\Gamma}'} \approx |V_{L',k'}|^{-1} B^D_{L',k'} := \sum_{j' \in \mathcal{N}(k')} |\Gamma^{L'}_{k'j'}| \, G^D(R_{L',k'}, R_{L',j'}, n_{k'j'}). \tag{3.21}$$

Here $\mathcal{N}(k')$ is the set of cells that have a common edge with the cell $V_{L',k'}$, and for $j' \in \mathcal{N}(k')$ let $\Gamma^{L'}_{k'j'} := \partial V_{L',k'} \cap \partial V_{L',j'}$ be the interface between the cells $V_{L',k'}$ and $V_{L',j'}$ and $n_{k'j'}$ the outer normal of $\Gamma^{L'}_{k'j'}$ corresponding to the cell $V_{L',k'}$. Furthermore the numerical flux function $F^I(U, W, n)$ and $F^D(U, W, n)$ are approximations for the inviscid and dissipative fluxes in normal direction n.

Model approximation: In order to discretize the model flux F^S in (3.20) we have to specify first the fluctuation of $\bar{\phi}'$. Since for the test function we use the box wavelet (3.11), it is determined by (3.12) as

$$\phi' = \tilde{\phi}_{L',k'} - \tilde{\phi}_{\bar{L},\bar{k}}, \quad V_{L',k'} \subset V_{\bar{L},\bar{k}}, \tag{3.22}$$

i.e., the fluctuation is just the difference of the fine-scale and coarse-scale box function (3.5). This is in agreement with (2.12). Note that it coincides with Gravemeier's choice

of fluctuation in [8]. Then we may rewrite the model term in (3.20) as

$$\langle \nabla \cdot F^S(U'), \phi' \rangle_\Omega = \langle \nabla \cdot F^S(U'), \tilde{\phi}_{L',k'} \rangle_\Omega - \langle \nabla \cdot F^S(U'), \tilde{\phi}_{\bar{L},\bar{k}} \rangle_\Omega. \tag{3.23}$$

The fluctuations U' of each of the conserved quantities are determined by the multiscale decomposition (2.10), where the coarse-scale contribution $\bar{U}$ is determined by the projection of $\bar{U}'$ to the scale $\bar{L}$. Then the model flux $F^S(U')$ can be determined by applying the Favre averaging (2.18) to compute the fluctuations of the velocity and temperature. Again we apply Gauss' theorem to (3.23) and obtain

$$\langle \nabla \cdot F^S(U'), \phi' \rangle_\Omega = \langle F^S(U') \cdot n, \tilde{\phi}_{L',k'} \rangle_{\bar{\Gamma}'} - \langle F^S(U') \cdot n, \tilde{\phi}_{\bar{L},\bar{k}} \rangle_{\bar{\Gamma}}, \tag{3.24}$$

where $\bar{\Gamma}'$ and $\bar{\Gamma}$ denote the boundaries of the supports of ϕ' and $\tilde{\phi}_{\bar{L},\bar{k}}$, respectively. In order to compute the gradients of these fluctuation terms we apply the same reconstruction techniques to the *fluctuation terms*. Note that in [8] the gradients of the fluctuations are rewritten employing the Favre averaging as the difference of gradients of the coarse-scale and fine-scale quantities, i.e.. $\nabla f' = \nabla \bar{f}' - \nabla \bar{f}$. Since the reconstruction process in general is nonlinear, the commutation between reconstruction and the Favre averaging remains to be proven. The first term on the right-hand side in (3.24) is thus approximated by

$$\langle F^S(U') \cdot n, \tilde{\phi}_{L',k'} \rangle_{\bar{\Gamma}'} \approx |V_{L',k'}|^{-1} B^{S,f}_{L',k'} := \sum_{j' \in \mathcal{N}(k')} |\Gamma^{L'}_{k'j'}| \, G^S(R'_{L',k'}, R'_{L',j'}, n_{k'j'}), \tag{3.25}$$

where $R'_{L',k'}$ denotes the reconstruction polynomial determined by the fluctuations of the primitive variables. For the second term we employ the two-scale relation (3.6) for the box functions. By the linearity of the integrals we then conclude

$$\langle F^S(U') \cdot n, \tilde{\phi}_{\bar{L},\bar{k}} \rangle_{\bar{\Gamma}} = \sum_{V_{L',r'} \subset V_{\bar{L},\bar{k}}} \frac{|V_{L',r'}|}{|V_{\bar{L},\bar{k}}|} \langle F^S(U') \cdot n, \tilde{\phi}_{L',r'} \rangle_{\bar{\Gamma}'}. \tag{3.26}$$

Note that those parts of the boundary integrals corresponding to $\bar{\Gamma}' = \partial V_{L',r'}$ lying inside the cell $V_{\bar{L},\bar{k}}$ cancel. Thus the second term on the right-hand side in (3.24) can be computed by averaging the first term on the right-hand side, i.e.,

$$\langle F^S(U') \cdot n, \tilde{\phi}_{\bar{L},\bar{k}} \rangle_{\bar{\Gamma}} \approx |V_{\bar{L},\bar{k}}|^{-1} B^{S,c}_{\bar{L},\bar{k}} := |V_{\bar{L},\bar{k}}|^{-1} \sum_{V_{L',r'} \subset V_{\bar{L},\bar{k}}} B^{S,f}_{L',r'}. \tag{3.27}$$

Summarizing (3.25) and (3.27) we finally obtain the discretization

$$\langle \nabla \cdot F^S(U'), \phi' \rangle_\Omega \approx |V_{L',k'}|^{-1} B^S_{L',k'} := |V_{L',k'}|^{-1} \left(B^{S,f}_{L',k'} - \frac{|V_{L',k'}|}{|V_{\bar{L},\bar{k}}|} B^{S,c}_{\bar{L},\bar{k}} \right) \tag{3.28}$$

of the model term in (3.17).

Time discretization: Finally we obtain the semi-discrete FV-VMS method

$$\frac{d}{dt} U_{L',k'} = -|V_{L',k'}|^{-1} \left(B^I_{L',k'} - B^D_{L',k'} - B^S_{L',k'} \right), \tag{3.29}$$

where we replace the terms in (3.17) by their approximations (3.19), (3.20), (3.25) and (3.27). For the time discretization we then apply some explicit Runge-Kutta method, where we use a global time step τ^n for all cells that might change due to the Courant-Friedrich-Levy (CFL) condition, i.e., $t^{n+1} = t^n + \tau^{n+1}$, $t^0 = 0$. Since the key ingredient of a Runge-Kutta scheme is a forward Euler step, we confine ourselves in the following

to the full discretization

$$U^{n+1}_{L',k'} = U^n_{L',k'} - \lambda^n_{L',k'} \left(B^{I,n}_{L',k'} - B^{D,n}_{L',k'} - B^{S,n}_{L',k'} \right), \quad \lambda^n_{L',k'} := \frac{\tau^n}{|V_{L',k'}|}. \tag{3.30}$$

Finally we have to comment on the choice of L and L'. So far, these parameters are fixed in our computations. In particular, it is not clear how to choose L'. From a conceptual point of view, it would be preferable to have some a posteriori control by which we can adapt the parameter locally during runtime. A reasonable criterion would be to control the effect of the unresolved small scales on the resolved scales such that (2.20) locally holds true. We will discuss this issue in more detail in Section 4.

3.3. *Adaptive multiresolution finite volume discretization of the VMS method*

The rationale behind the design of an adaptive multiresolution finite volume scheme of the VMS method (MR-FV-VMS) is to accelerate the FV scheme (3.30) (reference scheme) on a uniformly refined mesh (reference mesh) by computing actually *only* on a locally refined adapted subgrid, while preserving (up to a fixed constant multiple) the accuracy of the discretization on the full uniform grid. We shall briefly indicate now how to realize this strategy with the aid of the ingredients discussed in the previous sections.

The conceptual starting point is to rewrite the evolution equations for the cell averages $U_{L',k'}$, $k' \in I_{L'}$, of the reference scheme in terms of evolution equations for the multiscale coefficients. For this purpose we apply the discrete multiscale transformation (3.14) for the cell averages to the set of discrete evolution equations (3.30)

$$U^{n+1}_{l,k} = U^n_{l,k} - \lambda^n_{l,k} \left(B^{I,n}_{l,k} - B^{D,n}_{l,k} - B^{S,n}_{l,k} \right), \quad \lambda^n_{l,k} := \frac{\tau^n}{|V_{l,k}|}. \tag{3.31}$$

Here the flux balances $B^{*,n}_{l,k}$ corresponding to each of the three contributions are recursively defined by

$$B^{*,n}_{l,k} := \sum_{r \in \mathcal{M}^0_{l,k}} \frac{|V_{l,k}|}{|V_{l+1,r}|} m^{l,0}_{r,k} B^{*,n}_{l+1,r} = \sum_{r \in \mathcal{M}^0_{l,k}} B^{*,n}_{l+1,r}, \tag{3.32}$$

where we use (3.4) and (3.6). Due to the conservation property of the numerical fluxes, i.e., $G^*(U,W,-n) = -G^*(W,U,n)$, the internal fluxes in (3.32) cancel and, thus, the flux balances can be computed by the numerical fluxes at the boundary of the cell $V_{l,k}$

$$B^{*,n}_{l,k} = \sum_{\Gamma^l_{k,j} \subset \partial V_{l,k}} |\Gamma^l_{k,j}| G^{*,n,l}_{k,j}, \tag{3.33}$$

where $\Gamma^l_{k,j} := \partial V_{l,k} \cap \partial V_{l,j}$ denotes the common boundary segment of the two adjacent cells $V_{l,k}$ and $V_{l,j}$. In particular, we obtain the recursive formulae

$$G^{*,n,l}_{k,j} = \sum_{\Gamma^{L'}_{k',j'} \subset \Gamma^l_{k,j}} G^{*,n,L'}_{k',j'} \tag{3.34}$$

for the local numerical fluxes that are computed by the numerical fluxes of the *finest* scale L'. Note that in our computations we will employ

$$G^{*,n,l}_{k,j} = G^*(R^n_{l,k}, R^n_{l,j}, n_{k,j}), \tag{3.35}$$

where the reconstruction polynomials are determined by the local data of the adaptive

grid at time level t^n instead of the data of the finest refinement level. This has been justified in [21].

It is worthwhile mentioning that because of (3.32) and (3.25), (3.27) we conclude for the balances corresponding to the model term

$$B^{S,n}_{\bar{L},\bar{k}} := \sum_{V_{L',k'} \subset V_{\bar{L},\bar{k}}} B^{S,n}_{L',k'} = \sum_{V_{L',k'} \subset V_{\bar{L},\bar{k}}} \left(B^{S,f,n}_{L',k'} - \frac{|V_{L',k'}|}{|V_{\bar{L},\bar{k}}|} B^{S,c,n}_{\bar{L},\bar{k}} \right) = 0. \tag{3.36}$$

Here we use the nestedness of the grid hierarchy, i.e., $\sum_{V_{L',k'} \subset V_{\bar{L},\bar{k}}} |V_{L',k'}|/|V_{\bar{L},\bar{k}}| = 1$. Hence, there is *no* modeling term in (3.31) on coarser scales, i.e.,

$$B^{S,n}_{l,k} = 0, \quad l \leq \bar{L}. \tag{3.37}$$

Similarly, we derive evolution equations for the details, where we recursively apply the two-scale transformation for the details (3.14) to the evolution equations (3.30) of the cell averages for $l = L-1 \searrow 0$. Then the evolution process (3.30) on the uniform reference mesh is equivalent to the evolution of the multiscale coefficients, i.e., coarse-scale averages and details,

$$U^{n+1}_{0,k} = U^n_{0,k} - \lambda^n_{0,k} \left(B^{I,n}_{0,k} - B^{D,n}_{0,k} - B^{S,n}_{0,k} \right), \tag{3.38}$$

$$D^{n+1}_{l,k} = D^n_{l,k} - \sum_{r \in \mathcal{M}^1_{l,k}} m^{l,1}_{r,k} \, \lambda^n_{l+1,k} \left(B^{I,n}_{l+1,k} - B^{D,n}_{l+1,k} - B^{S,n}_{l+1,k} \right). \tag{3.39}$$

Here $D^n_{l,k}$ is a vector containing the details corresponding to all conservative quantities. By means of thresholding we now reduce the number of evolution equations to be solved. For this purpose, we construct a locally refined grid corresponding to some index set $\mathcal{G} \subset \{(l,k)\,;\, k \in \mathcal{I}_l,\ l = 0, \ldots, L'\}$, i.e., $\Omega = \bigcup_{(l,k)\in\mathcal{G}} V_{l,k}$. Equivalently, we can determine some index set $\mathcal{D} \subset \{(0,k)\,;\, k \in \mathcal{I}_0\} \cup \{(l,k)\,;\, k \in \mathcal{J}_l,\ l = 0, \ldots, L'-1\}$. Then the evolution equations (3.31) and (3.38), (3.39) are only solved on $\mathcal{G}$ and $\mathcal{D}$, respectively.

3.4. *Multiresolution-based grid adaptation*

In order to improve the efficiency of the reference scheme (3.30) we use multiresolution-based grid adaptation techniques. Here the refinement criterion is *not* based on a posteriori error estimates, typically not available for compressible flow equations, or residual-based criteria that do not allow for error control. Instead, we perform a multiscale analysis of the discrete data and apply threshold techniques to compress the data. In the following we briefly summarize the basic conceptual ideas.

Step 1: Multiscale analysis. Let $\mathbf{u}^n_{L'}$ be the cell averages representing the discretized flow field at some fixed time step t^n on a given locally refined grid with highest level of resolution $l = L'$. This sequence is encoded in arrays of *detail coefficients* $\mathbf{d}^n_l$, $l = 0, \ldots, L'-1$ of ascending resolution, see Figure 4, and cell averages on some coarsest level $l = 0$. For this purpose the multiscale transformation (3.14) needs to be performed *locally* which is possible due to the locality of the mask coefficients.

Step 2: Thresholding. It can be shown that the detail coefficients become small with increasing refinement level when the underlying function is smooth. In particular, the details (2.6) can be estimated by

$$\langle u, \tilde{\psi}_{l,k} \rangle_\Omega \leq \inf_{P \in \Pi_{M-1}} |\langle u - P, \tilde{\psi}_{l,k} \rangle_\Omega| \leq \inf_{P \in \Pi_{M-1}} \|u - P\|_{L^\infty(S_{l,k})} \leq C\, 2^{-M\,l} \|u\|_{W^{\infty,M}(S_{l,k})} \tag{3.40}$$

for any function u in the Sobolev space $W^{\infty,M}$ defined on the support $S_{l,k} := \operatorname{supp} \tilde{\psi}_{l,k}$ of the wavelet $\tilde{\psi}_{l,k}$, cf. [22]. Here we use the cancellation property (3.9). This motivates to neglect all sufficiently small details in order to compress the original data. Obviously, the compression rate will increase, if the decay $2^{-M\,l}$ can be improved. Therefore we use for the ansatz space the modified box wavelets realizing higher vanishing moments instead of the box wavelet. In order to compress the original data we now discard all detail coefficients $d^n_{l,k}$ whose absolute values fall below a level-dependent threshold value $\epsilon_l = 2^{l-L'}\epsilon$. Let

$$\mathcal{D}^n_{L,\epsilon} := \left\{(l,k)\ ;\ |d^n_{l,k}| > \varepsilon_l,\ k \in \mathcal{J}_l,\ l \in \{0,\ldots,L'-1\}\right\}$$

be the set of *significant details*. The ideal strategy would be to determine the threshold value ϵ such that the *discretization error* of the reference scheme, i.e., difference between exact solution and reference scheme, and the *perturbation error*, i.e., the difference between the reference scheme and the adaptive scheme, are balanced. For a detailed treatment of this issue we refer to [14, 21].

Step 3: Prediction and grading. Since the flow field evolves in time, grid adaptation is performed after each evolution step to provide the adaptive grid at the *new* time step. In order to guarantee the adaptive scheme to be *reliable* in the sense that no significant future feature of the solution is missed, we have to *predict* all significant details at the new time step $n+1$ by means of the details at the *old* time step n. Let $\tilde{\mathcal{D}}^{n+1}_{L,\epsilon}$ be the prediction set satisfying the *reliability condition*

$$\mathcal{D}^n_{L',\epsilon} \cup \mathcal{D}^{n+1}_{L',\epsilon} \subset \tilde{\mathcal{D}}^{n+1}_{L',\epsilon}. \tag{3.41}$$

Basically there are two prediction strategies (i.e. ways of choosing $\tilde{\mathcal{D}}^{n+1}_{L,\epsilon}$) discussed in the literature, see [14, 15]. Moreover, in order to perform the grid adaptation process, this set is additionally inflated somewhat such that the grid refinement history, i.e., the parent-child relations of subdivided cells, corresponds to a *graded* tree. Then the set of significant details can be interpreted as a graph where all details are connected by an edge in the graph.

Note that so far the prediction strategy only takes into account the transport of information. Since we are using an explicit time discretization and high Reynolds numbers, the effect due to dissipation will stay local as well and does not require an additional inflation of the prediction set. Moreover, it would be worthwhile to investigate the effect of the modeling terms employing the wavelets in order to control locally the choice of $\bar{L}$ and L' during the computation. In Section 4 we will discuss this issue in more detail.

Step 4: Grid adaptation. By means of the set $\tilde{\mathcal{D}}^{n+1}_{L',\epsilon}$ a locally refined grid is determined along the following lines. We check for the transformed flow data represented on $\tilde{\mathcal{D}}^{n+1}_{L',\epsilon}$ proceeding levelwise from coarse to fine whether the detail associated with any cell marked by the prediction set is significant or not. If it is, we refine the respective cell. We finally obtain the locally refined grid with hanging nodes represented by the index set $\tilde{\mathcal{G}}^{n+1}_{L',\epsilon}$. The flow data on the new grid can be computed from the detail coefficients in the same loop where we locally apply the inverse multiscale transformation (3.15).

4. Open Questions

In smooth, laminar regions, the resolved scales of the flow field may have small detail coefficients, due to the compression property of the wavelets. This can be exploited by the use of a locally coarsened grid and can be accounted for as an small additional

discretization error of the resolved scales. On the other hand, in regions with strong turbulence, we cannot expect a decay of the detail coefficients, resulting in the need of refining up to the highest level to calculate the modeled equation.

At the same time, we use a turbulence model. Usually these turbulence models contain parameters that allow the user to tune the model for a given test case, until good agreement with reference data is achieved. Therefore, each model is most suitable in the special situation it was designed for, e.g. fully developed isotropic turbulence. If we can detect such a region in our computational domain, we may be able to reduce the number of scales needed in the computation of the small resolved scales.

A similar approach is used in [23] for the LES, where the authors relate the decay of the detail coefficients of a suitable quantity calculated from the flow field with the decay rate of the energy spectrum $E(k)\tilde{k}^{-5/3}$ in the equilibrium range. If, locally, the actual decay rate does not match this predicted value, the authors conclude that the hypotheses of the turbulence model in use is not fulfilled. In that case, the grid has to be refined.

In the future, we would like to proceed similarly. For this purpose, we first must identify flow regimes, where the large scale quantities are in good agreement with reference data. In these regimes we have to analyze the behavior of the detail coefficients in order to develop an indicator that can mark flow regions, where the turbulence models works well. This has to be integrated in the grid refinement strategy, where we do not only account for discretization errors, but for modeling errors as well.

Acknowledgments

Financial support has been provided by the German Research Foundation (Deutsche Forschungsgemeinschaft – DFG) in the framework of the Sonderforschungsbereich Transregio 40.

References

[1] HUGHES, T.J.R., SCOVAZZI, G., BOCHEV, P.B. AND BUFFA, A. (2006). *A multiscale discontinuous Galerkin method with the computational structure of a continuous Galerkin method*. *Comput. Methods Appl. Mech. Engrg.*, **195**, 2761–2787.

[2] HUGHES, T.J.R., FEIJOO, G.R., MAZZEI, L. AND QUINCY, J.-B. (1998). *The variational multiscale method—a paradigm for computational mechanics*. *Comput. Methods Appl. Mech. Engrg.*, **166**, 3–24.

[3] ANDERSSON, U., ENGQUIST, B., LEDFELT, G. AND RUNBORG, O. (1999). *A contribution to wavelet-based subgrid modeling*. *Appl. Comput. Harmon. Anal.*, **7**, 151–164.

[4] JOHN, V. (2005). *An assessment of two models for the subgrid scale tensor in the rational LES model*. *J. Comput. Appl. Math.*, **173**, 57–80.

[5] BERSELLI, L.C., ILIESCU, T. AND LAYTON, W.J. (2006). *Mathematics of large eddy simulation of turbulent flows*. Scientific Computation. Springer-Verlag, Berlin.

[6] GUERMOND, J.-L., ODEN, J.T. AND PRUDHOMME, S. (2004). *Mathematical perspectives on large eddy simulation models for turbulent flows*. *J. Math. Fluid Mech.*, **6**, 194–248.

[7] LAYTON, W. (2002). *A connection between subgrid scale eddy viscosity and mixed methods*. *Appl. Math. Comput.*, **133**, 147–157.

[8] GRAVEMEIER, V. (2006). *Scale-separating operators for variational multiscale large eddy simulation of turbulent flows*. *J. Comp. Phys.*, **212**, 400–435.

[9] DUNCA, A., JOHN, V. AND LAYTON, W.J. (2004). The commutation error of the space averaged Navier-Stokes equations on a bounded domain. In: G.P. Galdi (Ed.) et al., *Contributions to current challenges in mathematical fluid mechanics. Basel: Birkhäuser. Advances in Mathematical Fluid Mechanics*, 53–78.

[10] COHEN, A., DAHMEN, W. AND DEVORE, R. (2003). *Adaptive wavelet schemes for nonlinear variational problems*. *SIAM J. Numer. Anal.*, **41**, 1785–1823.

[11] COHEN, A., DAHMEN, W. AND DEVORE, R. (2003). *Sparse evaluation of compositions of functions using multiscale expansions*. *SIAM J. Math. Anal.*, **35**, 279–303.

[12] CARNICER, J.M., DAHMEN, W. AND PEÑA, J.M. (1996). *Local decomposition of refinable spaces and wavelets*. *Appl. Comput. Harmon. Anal.*, **3**, 127–153.

[13] DAHMEN, W. (1994). Some remarks on multiscale transformations, stability and biorthogonality. In: P.J. Laurent, A. Le Méhauté and L.L. Schumaker (Eds.), *Wavelets, Images and Surface Fitting. Basel: AK Peters, Wellesley*, 157–188.

[14] COHEN, A., KABER, S.M., MÜLLER, S. AND POSTEL, M. (2003). *Fully adaptive multiresolution finite volume schemes for conservation laws*. *Math. Comp.*, **72**(241), 183-225.

[15] HARTEN, A. (1995). *Multiresolution algorithms for the numerical solution of hyperbolic conservation laws*. *Comm. Pure Appl. Math.*, **48**(12), 1305–1342.

[16] KOOBUS, B. AND FARHAT, CH. (2004). *VMS decomposition for compressible Navier Stokes*. *Computer Methods in Applied Mechanics and Engineering*, **193**, 1367–1383.

[17] FRÖHLICH, J. (2006). *Large Eddy Simulation turbulenter Strömungen*, Teubner Verlag.

[18] BRAMKAMP, F., LAMBY, PH. AND MÜLLER, S. (2004). *An adaptive multiscale finite volume solver for unsteady an steady state flow computations*. *J. Comp. Phys.*, **197**, 460–490.

[19] MÜLLER, S. (2003). Adaptive Multiscale Schemes for Conservation Laws. Lecture Notes on Computational Science and Engineering, Vol. 27. Springer.

[20] COHEN, A., DAUBECHIES, I. AND FEAUVEAU, J. (1992). *Biorthogonal bases of compactly supported wavelets*. *Comm. Pure Appl. Math.*, **45**, 485–560.

[21] HOVHANNISYAN, N., MÜLLER, S. (2009). *On the stability of fully adaptive multiscale schemes for conservation laws using approximate flux and source reconstruction strategies*. *IMA Journal of Numerical Analysis*, DOI:10.1093/imanum/drp010.

[22] COHEN, A. (2000). *Wavelet Methods in Numerical Analysis*. In: P.G. Ciarlet, J.L. Lions (Eds.), *Handbook of Numerical Analysis VII. Amsterdam, Elsevier*, 417–711.

[23] LÉONARD, S., TERRACOL, M. AND SAGAUT, P. (2006). A wavelet-based adaptive mesh refinement criterion for large-eddy simulation. *Journal of Turbulence*, **7**, Paper 64, 25 pp. (electronic).